

Article

Vapor-Driven Crosslinked Hydroxypropyl- β -Cyclodextrin Electrospun Nanofibrous Membranes for Ultrafast Dye Removal

Xinmiao Xu, Yi Zhang, Yong Chen * and Yu Liu *

College of Chemistry, State Key Laboratory of Elemento-Organic Chemistry, Nankai University, Tianjin 300071, China

* Correspondence: chen Yong@nankai.edu.cn (Y.C.); yuliu@nankai.edu.cn (Y.L.)

Abstract: Traditional separation membranes used for dye removal often suffer from a trade-off between separation efficiency and water permeability. Herein, we propose a facile approach to prepare cyclodextrin-based high-flux nanofiber membranes by electrospinning and vapor-driven crosslinking processes. The application of glutaraldehyde vapor for crosslinking hydroxypropyl- β -cyclodextrin (HP- β -CD)/polyvinyl alcohol (PVA)/laponite electrospun membranes can build interconnected structures and lead to the formation of a porous hierarchical layer. In addition, the incorporation of inorganic salt, laponite, can alter the crosslinking process, resulting in membranes with improved hydrophilicity and highly maintained electrospun nanofibrous morphology, which contributes to an ultrafast water flux of $1.0 \times 10^5 \text{ Lh}^{-1} \text{m}^{-2} \text{bar}^{-1}$. Due to the synergetic effect of strong host-guest interaction and electrostatic interaction, the membranes exhibit suitable rejection toward anionic dyes with a high removal efficiency of >99% within a short time and achieve accurate separation for cationic against anionic dyes, accompanied by suitable recyclability with >97% separation efficiency after at least four separation-regenerations. The prepared membranes with remarkable separation efficiency and ultrafast permeation properties might be a promising candidate for high-performance membranes in water treatment.

Keywords: cyclodextrin; supramolecular adsorption; electrospinning; nanofibrous membranes; ultrafast permeation



Citation: Xu, X.; Zhang, Y.; Chen, Y.; Liu, Y. Vapor-Driven Crosslinked Hydroxypropyl- β -Cyclodextrin Electrospun Nanofibrous Membranes for Ultrafast Dye Removal. *Chemistry* **2024**, *6*, 506–516. <https://doi.org/10.3390/chemistry6040029>

Received: 22 May 2024

Revised: 19 June 2024

Accepted: 21 June 2024

Published: 25 June 2024



Copyright: © 2024 by the authors. Licensee MDPI, Basel, Switzerland. This article is an open access article distributed under the terms and conditions of the Creative Commons Attribution (CC BY) license (<https://creativecommons.org/licenses/by/4.0/>).

1. Introduction

Many synthetic organic dyes used in the food, cosmetics, leather, and textile industries are mutagenic and carcinogenic [1,2]. Aquatic ecosystems and human health are seriously threatened by the widespread release of dye effluents with the quick rise in industrialization [3]. It is very important to find efficient dye removal techniques for wastewater treatment. Numerous tactics, such as chemical oxidation [4], biological degradation [5], and adsorption [6,7], have been thoroughly studied. Among these, membrane separation technology has drawn more and more interest due to its affordability, convenience, and lack of pollution [8]. As a result, great efforts are made to create high-performance membranes that simultaneously have strong rejection and high flux [9,10].

β -cyclodextrin (β -CD), which is low-cost and sustainable, possesses the hydrophobic cavity to form stable inclusion complexes with certain organic molecules through host-guest interactions and is widely applied in pollutant adsorption [11–14]. In addition, employing the main building block of the membranes, the intrinsic microporosity of β -CD can achieve accurate separation through size exclusion and serve as an extra water transport channel [15,16]. Peinmann et al. developed a method with per-6-amino- β -CDs instead of diamine reacting with terephthaloyl chloride to form a cyclodextrin-based separation layer by interfacial polymerization, which showed precise shape-selective permeability and a water permeance of $20 \text{ Lm}^{-2} \text{h}^{-1} \text{bar}^{-1}$ [17]. However, these CD-based crosslinked membranes produced by traditional interfacial polymerization reactions in solution are still too dense to enable fast solvent transport [18–21].

General methods to coordinate the water permeability of the membranes include improving the membrane surface hydrophilicity [22,23], introducing a water transfer channel [24,25], and increasing the specific surface area [26]. Electrospinning, as a versatile and economical method to produce nanofiber membranes with a high length–diameter ratio and adjustable morphology, has great potential in fields of air filtration [27] and water purification [28]. Native β -CD is hard to meet a certain viscosity for electrospinning, while hydroxypropyl β -CD (HP- β -CD) with much better solubility has been used for a non-polymeric electrospun system [29]. Several methods available to crosslink the water-soluble electrospun nanofibers include thermal crosslinking [30] and chemical crosslinking with crosslinking agents such as NHS/EDC [31,32]. There are several approaches to crosslink the water-soluble electrospun nanofibers, including chemical crosslinking with crosslinking agents like NHS/EDC [31,32] and thermal crosslinking [30], both of which require much energy and hazardous reagents. On the other hand, using glutaraldehyde (GA) vapor for crosslinking can significantly reduce operational complexity and eliminate the need for expensive and hazardous organic solvents like hexane, which improves convenience, accessibility, and sustainability [33–35]. More importantly, the vapor phase crosslinking is sufficiently gentle to preserve the water-soluble nanofibers' morphology to the fullest extent possible and create an interconnected structure, which increases the amount of water transport channels and expedites water flow [36–38].

Since the incorporation of inorganic salt can further improve the hydrophilicity, we also doped laponite, a cheap clay with negative disk-like surfaces and positive edges, into the membranes [39,40]. Herein, we electrospun HP- β -CD, PVA, and laponite on polyacrylonitrile (PAN)/polyethyleneimine (PEI) electrospinning substrate and employed GA vapor as crosslinking reagent to obtain multi-layer HP- β -CD crosslinked nanofiber (CD-CNF) membranes (Figure 1a). The relatively high content of HP- β -CD represented prominent adsorption capacity with strong host–guest interaction, while PVA was fixed at a low concentration to assist the HP- β -CD-dominated electrospinning process. The mass fraction of laponite to HP- β -CD was changed from 0, 1 wt%, 2 wt%, and 3 wt%, which produced four kinds of electrospun membranes, CD/PVA/Lap0, CD/PVA/Lap1%, CD/PVA/Lap2%, and CD/PVA/Lap3%, and the corresponding membranes after crosslinking were denoted as CD-CNF1, CD-CNF2, CD-CNF3, and CD-CNF4. Interestingly, the doped laponite had an effect on the electrospinning and further influenced the vapor-driven crosslinking stage. In the salt-mediated crosslinking process (Figure 1b,c), the existence of laponite would decrease the crosslinking reactivity and lead to the high maintenance of original electrospun nanofibers. In contrast to the compact structure of conventional filtration membranes, our nanofibrous membranes were expected to achieve ultrafast water flux.

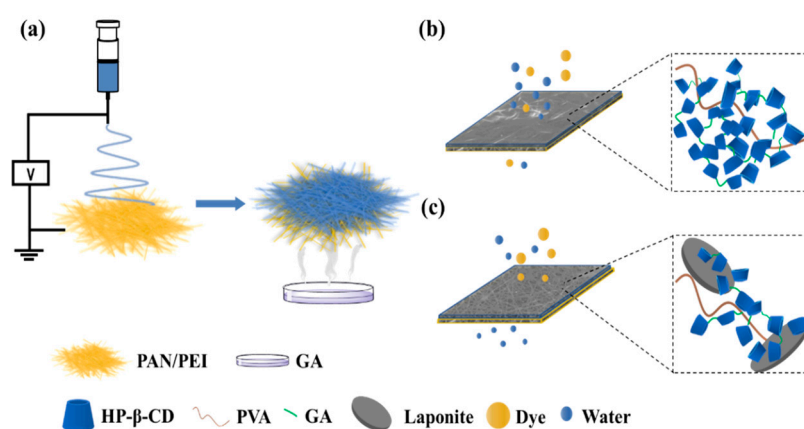


Figure 1. (a) Schematic illustration preparation of HP- β -CD nanofibrous membranes. Schematic illustration of the crosslinking and wastewater filtration process of CD-CNFs (b) without laponite and (c) with laponite.

2. Materials and Methods

2.1. Materials

All reagents were used without further purification. Polyacrylonitrile (PAN, average $M_w = 150,000$), polyethyleneimine (PEI, average $M_w = 45,000$, 50% aqueous solution), polyvinyl alcohol (PVA, 99% hydrolyzed, degree of polymerization = 1700), hydroxypropyl β -cyclodextrin (HP- β -CD, average substitution degree = 7, $M_w = 1541.54$), laponite, glutaraldehyde (GA, 25% aqueous solution), and bovine serum protein (BSA) were purchased from Macklin Reagent Co., Ltd. (Tianjin, China). Tropaeolin O, Indigo Carmine, Carmoisine, Direct Yellow 12, Reactive Black 5, Basic Red 2, Rhodamine B, Crystal Violet, and Thioflavine T were purchased from Aladdin Reagent Company.

2.2. Preparation of Nanofibrous Membranes

Electrospinning: 9.6% w/v PAN and 2.4% w/v PEI were dissolved in N, N-dimethylformamide (DMF) and stirred for 6 h at 80 °C to prepare a homogeneous solution. A total of 8 mL of the solution was loaded into a syringe equipped with a 20 gauge with a flow rate of 4 mLh⁻¹, and a high voltage (15 kV) was applied. The distance between the syringe and the aluminum (Al) foil-coated collector was 20 cm, and the cylindrical collector rotational speed was 125 rpm. A total of 1 g of HP- β -CD, 80 mg of PVA, and different weights of laponite, 0 mg, 10 mg, 20 mg, and 30 mg, corresponding to the weight ratio to HP- β -CD of 0, 1%, 2%, and 3%, were dissolved in 2 mL of deionized water and stirred overnight, respectively. The above solutions were transferred to the syringe with a 23 gauge and electrospun directly onto the PAN/PEI-coated Al foil. The voltage was set as 25 kV, and the flow rate was 1 mL h⁻¹. Depending on the proportion of laponite to HP- β -CD, the four kinds of membranes were denoted as CD/PVA/Lap0, CD/PVA/Lap1%, CD/PVA/Lap2%, and CD/PVA/Lap3%.

A total of 20 mL of GA solution (25% aqueous solution) in a petri dish was put in a vacuum desiccator, and the obtained electrospun nanofibers on Al foil were covered beyond the petri dish without touching the solution. After applying the vacuum for 24 h, the membranes were removed from the foil, washed with deionized water for several minutes, and vacuum-dried at 50 °C overnight. The crosslinked membranes were represented as CD-CNF1 (CD/PVA/Lap0), CD-CNF2 (CD/PVA/Lap1%), CD-CNF3 (CD/PVA/Lap2%), and CD-CNF4 (CD/PVA/Lap3%).

2.3. Characterization Methods

A field emission scanning electron microscope (Merlin Compact, Oberkochen, Germany) was used to acquire the surface morphologies of nanofibrous membranes. A thin layer of gold was applied to the coat to increase the conductivity. The acceleration voltage was 30 kV. The average diameters of fibers were measured with Image J software 1.46 r. A Fourier transform IR spectrometer (Bruker Tensor II, Ettlingen, Germany) was used to obtain the IR spectra of samples between 4000 and 400 cm⁻¹ under ambient temperature. X-ray photoelectron spectroscopy (XPS) was carried out on an instrument (Kratos Analytical Ltd.-Axis Ultra DLD, Manchester, UK) equipped with a monochromatized Al K α X-ray source. Data were analyzed with CASA XPS software (version number Casa2319PR1-0). Thermogravimetric Analysis (TGA) was performed on a thermogravimetric analyzer (NET-ZSCH, Selb, Germany) in the temperature range from 25 to 800 °C at a heating rate of 10 °C/min with N₂ as a purge gas at a flow rate of 25 mL min⁻¹. The water contact angle (WCA) was determined using a goniometer consisting of an analyzer (Dataphysics OCA20, Filderstadt, Germany). The surface charge of the membranes was evaluated by zeta potential analysis using a SurPASS 3 Electrokinetic Analyzer instrument.

2.4. Water Permeation Studies

The water sorption gravimetric method was used to evaluate the total porosity of the prepared membranes. The membranes were cut into 10 mm \times 10 mm pieces. The dried weight (W_d) was taken, and then the membranes were soaked in DI water for 24 h. After

lightly blotting the membrane surface with filter paper to remove water, the weight of the wet membranes (W_w) was taken. The water content percentage of the membranes was calculated using the formula

$$\text{Water content \%} = \frac{W_w - W_d}{W_d} \times 100 \quad (1)$$

After soaking in deionized water for 24 h, the membranes were cut down to 20 mm × 20 mm squares. The membranes were pre-pressurized for 10 min at 1 bar to stabilize the flux rate. Pure water and organic solvent, including ethyl alcohol, petroleum ether, and dichloromethane, were applied for performance analysis. The permeate flux rate (J) for all the prepared membranes was computed using Equation (2).

$$J = \frac{Q}{t * A} \quad (2)$$

where Q denotes the volume of permeated solute (in L), t is the time taken during permeation (in h), and A denotes the effective filtration area of membranes (in m^2).

2.5. Dye Filtration Experiments

A series of filtration experiments were performed with a dead-end sand core of a micro-solvent filter device using a vacuum pump. The five kinds of anionic dyes involved Indigo Carmine, Tropaeolin O, Reactive Black 5, Direct Yellow 12, and Carmoisine, and the four kinds of cationic dyes included Basic Red 2, Crystal Violet, Rhodamine B, and Thioflavine T. The effective area of membranes was 1.77 cm^2 . The concentration of the dye was fixed at 25 μM , and the feed solution volume was 5 mL. The recyclability of membranes was also evaluated using the above five kinds of anionic dyes (10 μM), and the feed solution was 20 mL each time. After filtration, the membranes were soaked in 1 mol/L NaOH solution, oscillated for 5 min, and rinsed with pure water several times. The filtration/regeneration cycles were repeated four times.

Anti-fouling experiments were conducted by using BSA aqueous solution (500 ppm) as a model foulant at 1 bar. A total of 40 mL 500 ppm BSA feed solution was applied each time to attain the permeate flux, and the membranes were washed with deionized water for one minute. The processes were repeated four times. The initial water flux was chosen as J_w , and the flux after one cycle was chosen as J_0 . The water flux after washing with pure water was denoted as $J_{w,1}$. The performance of all membranes was studied for 4 cycles. Using Equations (3) and (4), the flux values obtained were used to estimate the total fouling percentage (F_T)% and the recovery ratio percentage (F_{RR})%.

$$F_T(\%) = \left(\frac{J_w - J_0}{J_w} \right) \times 100 \quad (3)$$

$$F_{RR}(\%) = \frac{J_{w,1}}{J_w} \times 100 \quad (4)$$

3. Results

3.1. Structural and Morphological Characterizations of the CD-CNFs

The FTIR spectra of CD/PVA/Lap0, CD-CNF1, CD-CNF2, CD-CNF3, and CD-CNF4 membranes are presented in Figure 2a. The stretching vibration adsorption of Mg-OH from laponite emerged at 655 cm^{-1} in CD-CNF2, CD-CNF3, and CD-CNF4 membranes. In addition, the characteristic peak of 2240 cm^{-1} of $-C\equiv N$ in the substrate layer appeared in CD-CNF2, CD-CNF3, and CD-CNF4, caused by the laponite participating electrospinning process, which created surface defects. Except for CD/PVA/Lap0, a new peak at 2820 cm^{-1} appeared in CD-CNFs belonging to the stretching vibration of CH in the acetal linkage, and the O-H stretching adsorption at 3200–3600 cm^{-1} decreased, indicating that the hydroxyl groups in HP- β -CD and PVA reacted with aldehyde groups from GA. The peaks

at 1030 cm^{-1} , 1252 cm^{-1} , and 586 cm^{-1} ascribed to HP- β -CD were nearly unchanged, indicating that the characteristic structure of cyclodextrin still remained after crosslinking. After being treated by GA vapor, the adsorption peak at 1729 cm^{-1} attributing to the vibration peak for carbonyl arose, where the membrane without laponite (CD-CNF1) showed the highest intensity, demonstrating that the doped salt might impede the crosslinking process of the membrane. Moreover, in the FTIR results of PAN/PEI substrate before and after GA treatment (Figure S1), the peak attributed to the -NH group at 1561 cm^{-1} in PEI disappeared, suggesting that the crosslinking reaction occurs in the substrate membrane. In the TGA results (Figure 2b), the evaporation of solvents, including DMF and water, caused the weight loss below $300\text{ }^{\circ}\text{C}$. The mass loss peak at $367\text{ }^{\circ}\text{C}$ belonged to the decomposition temperature of HP- β -CD. All CD-CNF membranes were endowed with better thermal stability than CD/PVA/Lap0, and CD-CNF1 exhibited best considering the weight loss stage between $350\text{ }^{\circ}\text{C}$ and $400\text{ }^{\circ}\text{C}$. The results illustrated that the thermal stabilities of CD-CNFs decreased with increasing amounts of laponite.

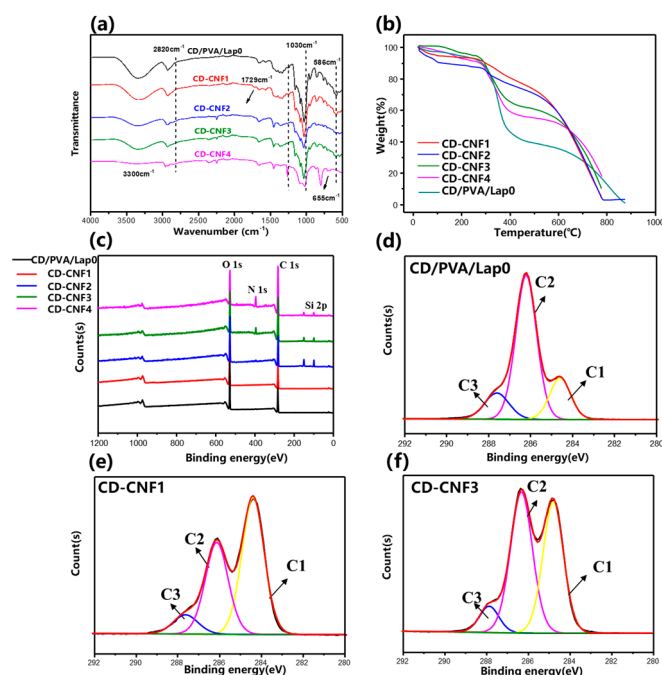


Figure 2. (a) FTIR spectra and (b) TGA curves of CD/PVA/Lap0 and CD-CNFs. (c) XPS wide scan spectra and C 1s core level deconvoluted XPS spectra for (d) CD/PVA/Lap0, (e) CD-CNF1, and (f) CD-CNF3 membranes, respectively. The groups that could be attributed to the C peak are C-C and C-H for C1, C-O, $\text{C}\equiv\text{N}$, C-N, and C=O for C2, and O-C-O for C3 [19].

In order to acquire insight into the crosslinking process, X-ray photoelectron spectroscopy was applied. The wide scan results of CD/PVA/Lap0 (Figure 2c) showed that in all membranes, the main peaks of C 1s and O 1s appeared at 285 eV and 532 eV. The element Si was detected at 150 eV and 99.7 eV on the membranes with the addition of laponite. Moreover, in CD-CNF3 and CD-CNF4, the binding energy peak at 400 eV assigned to the N element from the substrate emerged, confirming the existence of surface defects in the HP- β -CD layer. The deconvoluted C 1s XPS core level spectra of CD/PVA/Lap0 and CD-CNFs demonstrated (Figure 2d–f; Figure S3a,b) that after crosslinking, C1(C-C, C-H) peak intensity increased and C2(C-O) peak intensity declined in CD-CNF1. With the increasing content of laponite, the ratio of C1/C2 tended to decrease, indicating a lower crosslinking degree.

The crosslinking process had a direct impact on the morphology of the membranes. The scanning electron microscopy (SEM) results of HP- β -CD layers surface morphology before and after the GA vapor treatment are presented in Figure S4. With an elevated mass fraction of laponite to HP- β -CD, the diameter of electrospun nanofibers increased

(Figure S4e–h). Compared with the uniform nanofibers in CD/PVA/Lap0 (Figure 3a,b), the unsmooth nanofibers with bead structure appeared in CD/PVA/Lap2% by the aggregation of excessive salt, which might affect the membrane compatibility with the crosslinking agents. After the GA vapor-driven crosslinking, the fibrous structures of membranes were maintained to different extents. CD-CNF1 lost its original nanofiber morphology completely (Figure 3c), displaying as a compact surface layer without porosity, while there were many bulges attached to nanofibers and obvious minimum intersection in CD-CNF4 with the highest porosity (Figure S4). The most homogeneous morphology was presented in CD-CNF3 (Figure 3d), achieving the balance between fibrous and intermingled structures. Moreover, due to the limited content of PEI, the nanofiber structure of the substrate was well kept with slight fusion after crosslinking in the SEM images of PAN/PEI substrate before and after crosslinking (Figure S2). According to the cross-section SEM images (Figure 3e,f), both CD-CNF1 and CD-CNF3 membranes possessed multi-layer fibrous structures. In contrast to the conventional dense thin film, the membranes presented as 3D loose vesicular sponge structures with high porosity, providing abundant water transport channels. In the water uptake experiments, which represented the porosity of the membranes (Figure S7), the water content for CD-CNF1, CD-CNF2, CD-CNF3, and CD-CNF4 was measured as 14.6%, 26.1%, 54.7%, and 116.3%, respectively, indicating the increased membrane porosity. After soaking in water for three months, the morphology of PAN/PEI, CD-CNF1, and CD-CNF3 (Figure S6) did not change with little swelling, suggesting the suitable water stability of the membranes.

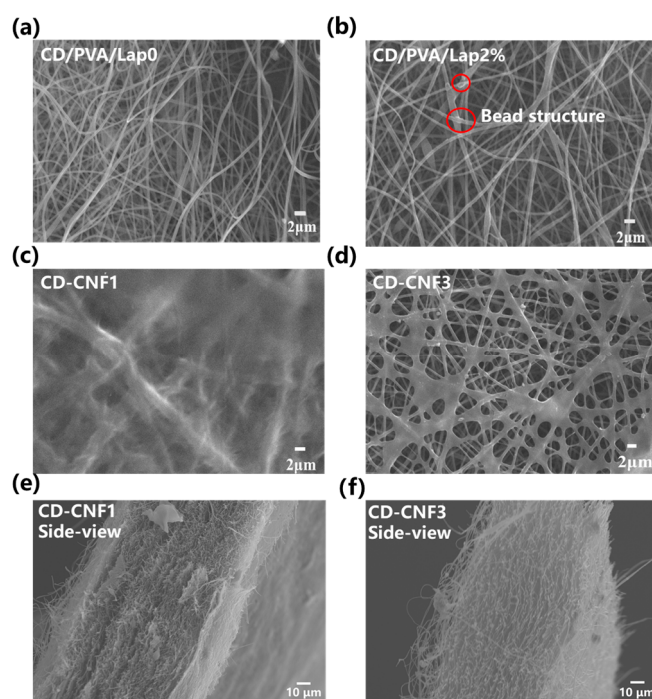


Figure 3. The SEM results of surface morphology of (a) CD/PVA/Lap0, (b) CD/PVA/Lap2%, (c) CD-CNF1, and (d) CD-CNF3 membranes. The cross-sectional images of (e) CD-CNF1 and (f) CD-CNF3 membranes.

3.2. Water Permeation and Dye Rejection Performance of the CD-CNFs

Hydrophilicity is also an important factor related to water permeability. The water contact angle of the PAN/PEI substrate and cyclodextrins-crosslinked layers was measured (Figure 4a). The results showed that all of the membranes were super hydrophilic as water droplets could not exist steadily on the surface and would infiltrate into the membranes within seconds or fewer. The water contact angle at the first 0.5 s was measured to be 104.3° for PAN/PEI substrate, 69.1° for CD-CNF1, 63.1° for CD-CNF2, 45.1° for CD-CNF3 and 51.5° for CD-CNF4. The surface roughness caused the hysteresis of the permeation, and

the water contact angle for CD-CNF4 was higher than for CD-CNF3. The above results demonstrated that the doped laponite could improve the hydrophilicity of the membranes.

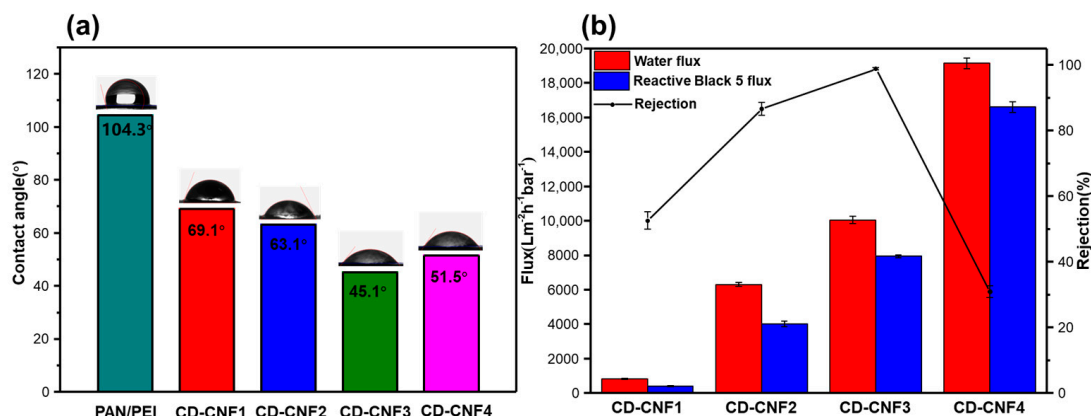


Figure 4. (a) The water contact angle of PAN/PEI, CD-CNF1, CD-CNF2, CD-CNF3, and CD-CNF4 membranes; (b) permeance of pure water, permeance and rejection of Reactive Black 5 solution (10^{-5} mol L⁻¹) of the CD-CNF1, CD-CNF2, CD-CNF3, and CD-CNF4 membranes.

Benefiting from the improved hydrophilicity and high porosity, CD-CNF membranes all exhibited surprisingly ultrafast water flux. The permeate flux of CD-CNF1, CD-CNF2, CD-CNF3, and CD-CNF4 for pure water was calculated to be 815 ± 45 , 6308 ± 118 , $10,047 \pm 221$, and $19,142 \pm 305$ Lh⁻¹m⁻²bar⁻¹, respectively (Figure 4b). The inherent cavity of cyclodextrin and the interconnected nanofibrous structure of the electrospun membrane both provided abundant transport channels and facilitated the water molecule speed-up passage. In addition, the CD-CNF flux for organic solvents was also high (Table S1). For example, the flux of the CD-CNF3 membrane for dichloromethane was $11,842$ Lh⁻¹m⁻²bar⁻¹. By applying the membranes for dye filtration, the CD-CNF3 membrane exhibited a flux up to 7942 ± 81 Lh⁻¹m⁻² bar⁻¹ for Reactive Black 5 solution (10^{-5} mol L⁻¹) with an excellent rejection beyond 99%.

The rejection performances of the CD-CNFs were further explored with five kinds of anionic dyes (Tropaeolin O, Indigo Carmine, Carmoisine, Direct Yellow 12, and Reactive Black 5) (Figure 5a). When the concentration of the dyes was fixed at 2.5×10^{-5} mol L⁻¹, CD-CNF3 membranes exhibited a removal efficiency of >99% against the above dyes with ultrafast permeation. For example, 20 mL of Carmoisine solution was filtrated to obtain colorless water by CD-CNF3 in 10 s (Figure 5b; Video S1). The two types of separation mechanisms are electrostatic effect and molecular sieving [37]. Molecular sieving included the cavity from HP- β -CD and trapping through the nanofibrous structure's porosity. Because of its rapid transit and minimal interaction with contaminants, CD-CNF4, the least crosslinked of the three, exhibited a low dye rejection rate of between 30 and 60%. Notably, the cyclodextrin cavity's high affinity for the dye molecule's structure explained why CD-CNF1, CD-CNF2, and CD-CNF3 membranes all exhibited strong rejection against Tropaeolin O. (Figure S9a). The surface charge was determined by zeta potential analysis. At pH 7, all of the membranes were positively charged (Figure S10). The CD-CNF4 was less positively charged because of the agglomeration of the clay. CD-CNF1 and CD-CNF2 membranes with less electrostatic interaction (less laponite) exhibited a moderate rejection rate of around 80% toward other dyes, whereas in CD-CNF3, salt-mediated crosslinking interconnected structure and electrostatic interaction realized a consummate balance, leading to the remarkable removal rate and the ultrafast flux at the same time.

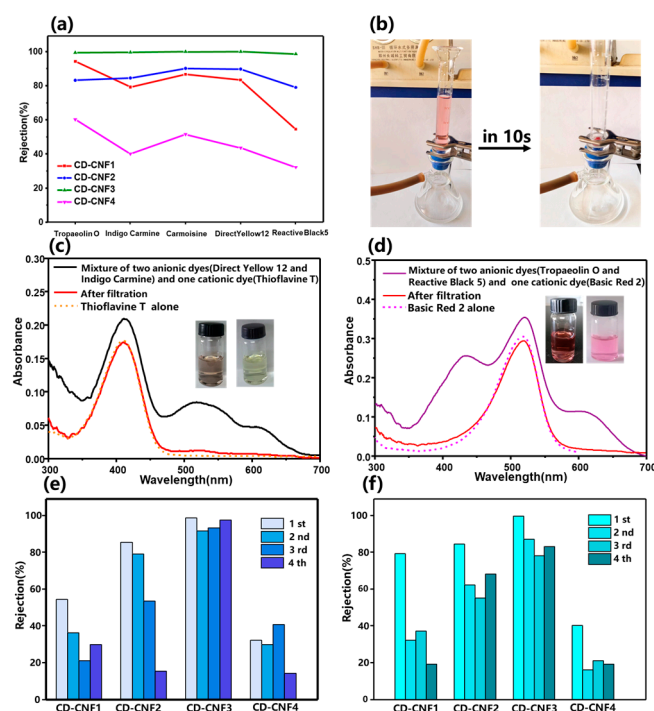


Figure 5. (a) Rejection of CD-CNFs toward Tropaeolin O, Indigo Carmine, Carmoisine, Direct Yellow 12, and Reactive Black 5 solution (the concentration of dyes was fixed at 2.5×10^{-5} mol L⁻¹); (b) equipment of filtration and photograph of Carmoisine (10^{-5} mol L⁻¹) before and after filtration; UV-Vis spectrum of mixture of Direct Yellow 12 (5×10^{-6} mol L⁻¹), Indigo Carmine (5×10^{-6} mol L⁻¹), and Thioflavine T (10^{-5} mol L⁻¹) before and after filtration with CD-CNF3 film; (c) UV-Vis spectrum of 10^{-5} mol L⁻¹ pure Thioflavine T solution; (d) UV-Vis spectrum of mixture of Reactive Black 5 (5×10^{-6} mol L⁻¹), Tropaeolin O (5×10^{-6} mol L⁻¹), and Basic Red 2 (10^{-5} mol L⁻¹) before and after filtration with CD-CNF3 film; (e) UV-Vis spectrum of 10^{-5} mol L⁻¹ pure Basic Red 2 solution, the rejection of CD-CNF membranes toward (e) Reactive Black 5 and (f) Indigo Carmine in four filtration/regeneration cycles.

Moreover, owing to the electrostatic repulsion interaction, the membranes showed lower rejection properties toward cationic dyes (Figure S11). Therefore, the membranes can be used for the separation of cationic and anionic dyes. The separation ability of CD-CNF3 was tested using dye mixtures, including two kinds of anionic dyes and one kind of cationic dye. The membrane had excellent rejection for two anionic dyes (Direct Yellow 12, Indigo Carmine) while leaving nearly all of the cationic dye (Thioflavine T) in the filtrate (Figure 5c). Similar results were obtained with different kinds of mixed dyes of Reactive Black 5, Tropaeolin O, and Basic Red 2 (Figure 5d). The CD-CNF3 also showed rapid separation, as shown in the video, that 10 mL of dye mixture solution could pass through the membrane in 8 s (Video S2). The membranes after dye filtration could be simply washed with NaOH solution and reused. After four cycles of filtration–regeneration (Figure 5e,f), the membranes still exhibited a rejection of 97.4% toward Reactive Black 5. Moreover, the CD-CNF3 membrane also presented suitable rejection for three other anionic dyes in four filtration/regeneration cycles (Figure S12), with a rejection of 98% toward Tropaeolin O after four filtration cycles, demonstrating the universal recyclability of the membranes for the filtration of anionic dyes.

3.3. The Anti-Fouling Properties of the CD-CNFs

Commercial separation membranes with inherent hydrophobicity frequently experience biomacromolecule fouling [34]. However, the surface hydrophilicity of our reported membranes was significantly increased. It was studied how the volume of BSA solution affected the penetration of the membrane using BSA as a model biomacromolecule pollu-

tant. With the increase in hydrophilicity, the CD-CNF3 and CD-CNF4 membranes were less contaminated with a lower total fouling ratio (Figure 6a), and the CD-CNF3 membrane showed suitable flux recovery as the normalized water flux remained at 68% (F_{RR}) after three cycles (Figure 6b). According to the surface morphology of CD-CNFs, as for CD-CNF1 without laponite (Figure 6c), the macromolecular pollutant is stacked tightly on the surface. However, there were just a few fibers attached to the pollutant on the surface of CD-CNF3 (Figure 6d) because the BSA has low compatibility with the hydrophilic membranes and was easily washed away from the membrane surface. The above results confirmed that the CD-CNF3 membranes had suitable anti-fouling abilities.

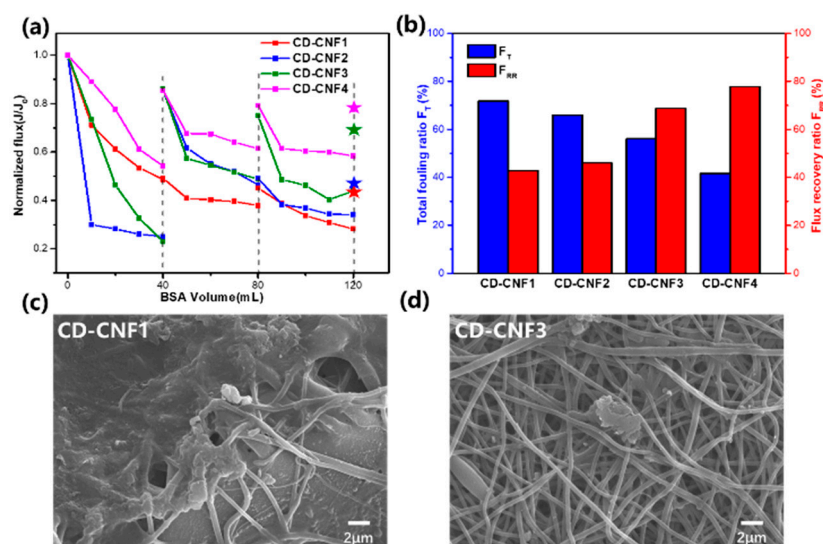


Figure 6. (a) Normalized flux of CD-CNFs changing with the treatment of different volumes of BSA (500 ppm), in which the dashed line represented rinsing the membranes with pure water; (b) F_T (total fouling ratio) and F_{RR} (Flux recovery ratio) of CD-CNFs in three cycles. The final SEM images of (c) CD-CNF1 and (d) CD-CNF3 membranes after BSA solution treatment and washing with water.

4. Discussion

In summary, crosslinked nanofiber membranes composed of HP- β -CD, PVA, and laponite were successfully prepared by electrospinning and GA vapor-driven crosslinking process. We found that the CD-CNF3 membrane (crosslinked CD/PVA/Lap2% membrane) possessed outstanding rejection for anionic dyes with an ultrafast water permeance of $10,047 \text{ Lh}^{-1}\text{m}^{-2}\text{bar}^{-1}$. The intrinsic cavity of cyclodextrin and the nanofibrous structure produced by the electrospinning and the salt-mediated vapor crosslinking process provided the membranes with abundant water transport channels, jointly achieving the ultrafast separation of dye wastewater. Due to the combination of supramolecular adsorption of HP- β -CD and electrostatic interaction replenished by laponite, the CD-CNF3 membrane exhibited a remarkable rejection rate of more than 99% against several anionic dyes and high-efficiency separation of cationic and anionic dyes. Moreover, the super hydrophilicity of the surface contributed to the suitable anti-fouling properties, leading to better recyclability. Moreover, the membranes with ultrafast separation ability are low-cost and easy to prepare, which have great potential application in dye sewage treatment.

Supplementary Materials: The following supporting information can be downloaded at <https://www.mdpi.com/article/10.3390/chemistry6040029/s1>, Figure S1: FTIR spectra of substrate membranes; Figure S2: SEM of substrate membranes; Figure S3: C 1s core level deconvoluted XPS spectra for CD-CNF2 and CD-CNF4 membranes, respectively; Figure S4: SEM results and nanofiber diameter distribution of CD-CNFs; Figure S5: Cross-sectional images of CD-CNFs; Figure S6: The SEM results of the membranes after soaking in water; Figure S7: The water content of CD-CNFs membranes; Figure S8: Photographs of prepared membranes after filtration; Figure S9: UV-Vis spectrum of anionic dyes after CD-CNFs filtration; Figure S10: The surface zeta potential of the CD-CNFs at pH 7;

Figure S11: UV-Vis spectrum of cationic dyes after CD-CNFs filtration; Figure S12: The rejection of CD-CNF membranes for three dyes in four filtration/regeneration cycles; Table S1: Permeances of CD-CNFs for three kinds of organic solvents; Video S1: The filtration process of Carmoisine solution by CD-CNF3 membrane; Video S2: The separation of mixed dyes by CD-CNF3 membrane.

Author Contributions: Conceptualization, X.X. and Y.C.; methodology, X.X. and Y.Z.; validation, X.X.; formal analysis, X.X. and Y.Z.; investigation, X.X.; resources, X.X.; data curation, X.X.; writing—original draft preparation, X.X.; writing—review and editing, X.X., Y.C. and Y.L.; project administration, Y.C. and Y.L.; funding acquisition, Y.C. All authors have read and agreed to the published version of the manuscript.

Funding: This research was funded by the National Natural Science Foundation of China (grant no. 22131008), the Haihe Laboratory of Sustainable Chemical Transformation, and the Fundamental Research Funds for the Central Universities (Nankai University).

Data Availability Statement: The data presented in this study are available on request from the corresponding author.

Conflicts of Interest: The authors declare no conflicts of interest.

References

1. Lin, J.; Ye, W.; Xie, M.; Seo, D.H.; Luo, J.; Wan, Y.; Van der Bruggen, B. Environmental impacts and remediation of dye-containing wastewater. *Nat. Rev. Earth Environ.* **2023**, *4*, 785–803. [[CrossRef](#)]
2. Shanker, U.; Rani, M.; Jassal, V. Degradation of hazardous organic dyes in water by nanomaterials. *Environ. Chem. Lett.* **2017**, *15*, 623–642. [[CrossRef](#)]
3. Tkaczyk, A.; Mitrowska, K.; Posyniak, A. Synthetic organic dyes as contaminants of the aquatic environment and their implications for ecosystems: A review. *Sci. Total Environ.* **2020**, *717*, 137222. [[CrossRef](#)] [[PubMed](#)]
4. Samuchiwal, S.; Naaz, F.; Kumar, P.; Ahammad, S.Z.; Malik, A. Life cycle assessment of sequential microbial-based anaerobic-aerobic reactor technology developed onsite for treating textile effluent. *Environ. Res.* **2023**, *234*, 116545. [[CrossRef](#)] [[PubMed](#)]
5. Giannakis, S. A review of the concepts, recent advances and niche applications of the (photo) Fenton process, beyond water/wastewater treatment: Surface functionalization, biomass treatment, combatting cancer and other medical uses. *Appl. Catal. B Environ.* **2019**, *248*, 309–319. [[CrossRef](#)]
6. Yan, J.; Huang, Y.; Miao, Y.E.; Tjiu, W.W.; Liu, T. Polydopamine-coated electrospun poly(vinyl alcohol)/polyacrylic acid membranes as efficient dye adsorbent with good recyclability. *J. Hazard. Mater.* **2015**, *283*, 730–739. [[CrossRef](#)]
7. Leudjo Taka, A.; Fosso-Kankeu, E.; Pillay, K.; Yangkou Mbianda, X. Metal nanoparticles decorated phosphorylated carbon nanotube/cyclodextrin nanosponge for trichloroethylene and Congo red dye adsorption from wastewater. *J. Environ. Chem. Eng.* **2020**, *8*, 103602. [[CrossRef](#)]
8. Sarkar, P.; Modak, S.; Karan, S. Ultrasensitive and Highly Permeable Polyamide Nanofilms for Ionic and Molecular Nanofiltration. *Adv. Funct. Mater.* **2021**, *31*, 2007054. [[CrossRef](#)]
9. Zhang, L.; Guan, H.; Zhang, N.; Jiang, B.; Sun, Y.; Yang, N. A loose NF membrane by grafting TiO₂-HMDI nanoparticles on PES/ β -CD substrate for dye/salt separation. *Sep. Purif. Technol.* **2019**, *218*, 8–19. [[CrossRef](#)]
10. Karki, S.; Gohain, M.B.; Yadav, D.; Thakare, N.R.; Pawar, R.R.; Hazarika, S.; Ingole, P.G. Building rapid water transport channels within thin-film nanocomposite membranes based on 2D mesoporous nanosheets. *Desalination* **2023**, *547*, 116222. [[CrossRef](#)]
11. Xu, W.; Chen, Y.; Xu, W.; Wu, X.; Liu, Y. Electrospinning Oriented Self-Cleaning Porous Crosslinking Polymer for Efficient Dyes Removal. *Adv. Mater. Interfaces* **2020**, *7*, 2001050. [[CrossRef](#)]
12. Zhang, W.; Zheng, Z.; Lin, L.; Zhang, X.; Bae, M.; Lee, J.; Xie, J.; Diao, G.; Im, H.-J.; Piao, Y.; et al. Ultrafast Synthesis of Graphene-Embedded Cyclodextrin-Metal-Organic Framework for Supramolecular Selective Absorbency and Supercapacitor Performance. *Adv. Sci.* **2023**, *10*, 2304062. [[CrossRef](#)] [[PubMed](#)]
13. Zhang, S.; Zhou, J.; Li, H. Chiral Covalent Organic Framework Packed Nanochannel Membrane for Enantioseparation. *Angew. Chem. Int. Ed.* **2022**, *61*, e202204012. [[CrossRef](#)]
14. Zhang, S.; Boussouar, I.; Li, H. Selective sensing and transport in bionic nanochannel based on macrocyclic host-guest chemistry. *Chin. Chem. Lett.* **2021**, *32*, 642–648. [[CrossRef](#)]
15. Jiang, Z.; Dong, R.; Evans, A.M.; Biere, N.; Ebrahim, M.A.; Li, S.; Anselmetti, D.; Dichtel, W.R.; Livingston, A.G. Aligned macrocycle pores in ultrathin films for accurate molecular sieving. *Nature* **2022**, *609*, 58–64. [[CrossRef](#)] [[PubMed](#)]
16. Alsbaiee, A.; Smith, B.J.; Xiao, L.; Ling, Y.; Helbling, D.E.; Dichtel, W.R. Rapid removal of organic micropollutants from water by a porous β -cyclodextrin polymer. *Nature* **2016**, *529*, 190–194. [[CrossRef](#)] [[PubMed](#)]
17. Huang, T.; Puspasari, T.; Nunes, S.P.; Peinemann, K.-V. Ultrathin 2D-Layered Cyclodextrin Membranes for High-Performance Organic Solvent Nanofiltration. *Adv. Funct. Mater.* **2020**, *30*, 1906797. [[CrossRef](#)]
18. Zhu, B.; Shao, R.; Li, N.; Min, C.; Liu, S.; Xu, Z.; Qian, X.; Wang, L. Progress of cyclodextrin based-membranes in water treatment: Special 3D bowl-like structure to achieve excellent separation. *Chem. Eng. J.* **2022**, *449*, 137013. [[CrossRef](#)]

19. Villalobos, L.F.; Huang, T.; Peinemann, K.-V. Cyclodextrin Films with Fast Solvent Transport and Shape-Selective Permeability. *Adv. Mater.* **2017**, *29*, 1606641. [[CrossRef](#)]
20. He, Y.; Miao, J.; Jiang, Z.; Tu, K.; Yang, H.; Chen, S.; Zhang, L.; Zhang, R. Improving the anti-fouling property and permeate flux of hollow fiber composite nanofiltration membrane using β -cyclodextrin. *Sci. Rep.* **2019**, *9*, 12435. [[CrossRef](#)]
21. Mao, H.; Zhang, H.; Li, Y.; Xue, Y.; Pei, F.; Wang, J.; Liu, J. Tunable Solvent Permeation Properties of Thin Film Nanocomposite Membrane by Constructing Dual-Pathways Using Cyclodextrins for Organic Solvent Nanofiltration. *ACS Sustain. Chem. Eng.* **2015**, *3*, 1925–1933. [[CrossRef](#)]
22. Gozali Balkanloo, P.; Mahmoudian, M.; Hosseinzadeh, M.T. A comparative study between MMT-Fe₃O₄/PES, MMT-HBE/PES, and MMT-acid activated/PES mixed matrix membranes. *Chem. Eng. J.* **2020**, *396*, 125188. [[CrossRef](#)]
23. Wu, H.; Liu, Y.; Mao, L.; Jiang, C.; Ang, J.; Lu, X. Doping polysulfone ultrafiltration membrane with TiO₂-PDA nanohybrid for simultaneous self-cleaning and self-protection. *J. Membr. Sci.* **2017**, *532*, 20–29. [[CrossRef](#)]
24. Shen, L.; Cheng, R.; Yi, M.; Hung, W.-S.; Japip, S.; Tian, L.; Zhang, X.; Jiang, S.; Li, S.; Wang, Y. Polyamide-based membranes with structural homogeneity for ultrafast molecular sieving. *Nat. Commun.* **2022**, *13*, 500. [[CrossRef](#)]
25. Zhao, Q.; Liu, Y. Macrocyclic crosslinked mesoporous polymers for ultrafast separation of organic dyes. *Chem. Commun.* **2018**, *54*, 7362–7365. [[CrossRef](#)]
26. Xu, W.; Li, G.; Qu, H.; Ma, C.; Zhang, H.; Cheng, J.; Li, H. The Specific Removal of Perfluorooctanoic Acid Based on Pillar[5]arene-Polymer-Packed Nanochannel Membrane. *ACS Nano* **2023**, *17*, 19305–19312. [[CrossRef](#)]
27. Xu, W.; Chen, Y.; Liu, Y. Directional Water Transfer Janus Nanofibrous Porous Membranes for Particulate Matter Filtration and Volatile Organic Compound Adsorption. *ACS Appl. Mater. Interfaces* **2021**, *13*, 3109–3118. [[CrossRef](#)] [[PubMed](#)]
28. Zhang, W.; Chai, H.; Diao, G. Highly porous cyclodextrin functionalized nanofibrous membrane by acid etching. *Colloids Surf. A Physicochem. Eng. Asp.* **2019**, *582*, 123907. [[CrossRef](#)]
29. Celebioglu, A.; Uyar, T. Electrospinning of nanofibers from non-polymeric systems: Polymer-free nanofibers from cyclodextrin derivatives. *Nanoscale* **2012**, *4*, 621–631. [[CrossRef](#)]
30. Zhao, R.; Wang, Y.; Li, X.; Sun, B.; Wang, C. Synthesis of beta-Cyclodextrin-Based Electrospun Nanofiber Membranes for Highly Efficient Adsorption and Separation of Methylene Blue. *ACS Appl. Mater. Interfaces* **2015**, *7*, 26649–26657. [[CrossRef](#)]
31. Li, R.; Dou, J.; Jiang, Q.; Li, J.; Xie, Z.; Liang, J.; Ren, X. Preparation and antimicrobial activity of β -cyclodextrin derivative copolymers/cellulose acetate nanofibers. *Chem. Eng. J.* **2014**, *248*, 264–272. [[CrossRef](#)]
32. Tang, Y.-J.; Shen, B.-J.; Huang, B.-Q.; Zhan, Z.-M.; Xu, Z.-L. High permselectivity thin-film composite nanofiltration membranes with 3D microstructure fabricated by incorporation of beta cyclodextrin. *Sep. Purif. Technol.* **2019**, *227*, 115718. [[CrossRef](#)]
33. Shang, S.; Chiu, K.-L.; Jiang, S. Synthesis of immobilized polyvinyl alcohol/cyclodextrin eco-adsorbent and its application for the removal of ibuprofen from pharmaceutical sewage. *J. Appl. Polym. Sci.* **2017**, *134*, 44861. [[CrossRef](#)]
34. Ahmad, J.; Wen, X.; Li, F.; Wang, B. Novel triangular silver nanoparticle modified membranes for enhanced antifouling performance. *RSC Adv.* **2019**, *9*, 6733–6744. [[CrossRef](#)] [[PubMed](#)]
35. Wang, Q.; Ju, J.; Tan, Y.; Hao, L.; Ma, Y.; Wu, Y.; Zhang, H.; Xia, Y.; Sui, K. Controlled synthesis of sodium alginate electrospun nanofiber membranes for multi-occasion adsorption and separation of methylene blue. *Carbohydr. Polym.* **2019**, *205*, 125–134. [[CrossRef](#)] [[PubMed](#)]
36. Tian, H.; Yuan, L.; Wang, J.; Wu, H.; Wang, H.; Xiang, A.; Ashok, B.; Rajulu, A.V. Electrospinning of polyvinyl alcohol into crosslinked nanofibers: An approach to fabricate functional adsorbent for heavy metals. *J. Hazard. Mater.* **2019**, *378*, 120751. [[CrossRef](#)] [[PubMed](#)]
37. Yadav, D.; Karki, S.; Gohain, M.B.; Ingole, P.G. Development of micropollutants removal process using thin-film nanocomposite membranes prepared by green new vapour-phase interfacial polymerization method. *Chem. Eng. J.* **2023**, *472*, 144940. [[CrossRef](#)]
38. Gruppuso, M.; Iorio, F.; Turco, G.; Marsich, E.; Porrelli, D. Hyaluronic acid/lactose-modified chitosan electrospun wound dressings—Crosslinking and stability criticalities. *Carbohydr. Polym.* **2022**, *288*, 119375. [[CrossRef](#)] [[PubMed](#)]
39. Prasannan, A.; Udamsin, J.; Tsai, H.-C.; Wang, C.-F.; Lai, J.-Y. Robust underwater superoleophobic membranes with bio-inspired carrageenan/laponite multilayers for the effective removal of emulsions, metal ions, and organic dyes from wastewater. *Chem. Eng. J.* **2020**, *391*, 123585. [[CrossRef](#)]
40. Yang, X.; Lin, L.; Liu, Z.; Yang, J.; Cheng, Q.; Ma, W.; Xu, M.; Tang, F.; Wang, Q.; Li, X.; et al. Preparation of solvent-resistant polyimide membranes for efficient separation of dyes and salts via an “internal drive” strategy. *Sep. Purif. Technol.* **2024**, *332*, 125843. [[CrossRef](#)]

Disclaimer/Publisher’s Note: The statements, opinions and data contained in all publications are solely those of the individual author(s) and contributor(s) and not of MDPI and/or the editor(s). MDPI and/or the editor(s) disclaim responsibility for any injury to people or property resulting from any ideas, methods, instructions or products referred to in the content.